Low temperature epitaxial SiGe:P for gate-all-around n-channel metal-oxide-semiconductor devices

Yuta Fujimoto [1], Andriy Hikavyy [2, 3], Clement Porret [2], Erik Rosseel [2], Gianluca Rengo [2], and Roger Loo [2, 4]

[1] *Sony Semiconductor Solutions, 4-14-1 Asahi-cho Atsugi-shi, Kanagawa, Japan*

[2] *Imec, Kapeldreef 75, Leuven, Belgium*

[3] *Currently at SOITEC, 691 Chem. de Pré Fontaine, 31890 Bernin, France*

[4] *Ghent University, Department of Solid-State Sciences, Krijgslaan 281, building S1, 9000 Ghent, Belgium*

E-mail: yuta.fujimoto@sony.com

This study investigates the viability of $Si_{1-x}Ge_x$:P ($x \leq 0.3$) as a novel source/drain material for n-channel Metal-Oxide-Semiconductor for Gate-All-Around (GAA) transistor, addressing the challenges posed by the evolving semiconductor technology. Utilizing a reduced-pressure chemical vapor deposition system, undoped SiGe with low Ge contents were grown at temperatures ≤ 500°C. The addition and optimization of phosphorous doping using phosphine results in improved surface morphology and increased active carrier concentration. The study compares $Si_{1-x}Ge_x$:P with different silicon precursors and temperatures, emphasizing the potential for maintaining high growth rates at lower temperatures when using Si_3H_8. Ti / $Si_{1-x}Ge_x$:P stacks reveal a promising reduction in contact resistivity with decreasing the Ge content, particularly when incorporating thin Si:P cap layers at the Ti / $Si_{1-x}Ge_x$:P interface. This comprehensive study highlights the potential of $Si_{1-x}Ge_x$:P as an alternative material for advanced GAA transistor technologies, offering improved mobility and meeting the thermal budget requirements.

1. Introduction

With the miniaturization and evolution of complementary metal oxide semiconductor (CMOS) devices, the specifications of processes and materials are regularly updated. New device concepts such as Gate-All-Around (GAA) transistors and Complementary Field-Effect Transistors (CFET) are considered for technologies below the 2 nm node [1-4]. The considered designs bring new challenges, in particular for source/drain (S/D) engineering.

Strained channels have been employed from the 90 nm node, and are still being utilized in FinFET, which has become mainstream from the 22 nm node [5-7]. Currently, SiGe:B (pMOS) and Si:P (nMOS) are utilized for S/D engineering, in order to apply compressive and tensile strain in the Si channel, respectively. Moreover, the active carrier concentrations achieved in these materials amount to ~ 1×10^{21} cm^{-3} [8-12]. However, recent TCAD simulations have shown that SiGe:B and Si:P generate tensile and compressive strain in {110}-oriented GAA Si channels, respectively [13-14]. Therefore, employing conventional S/D materials in GAA architectures is expected to lead to channel strain inversion and mobility degradation. Hence, to attain the correct strain signs, leading to improved mobilities, we propose to use $Si_{1-x}Ge_x$:P ($x \leq 0.3$) for nMOS.

In addition, in sub 2 nm technology nodes, process temperatures below 500°C [1,2,15,16] and contact resistivities (ρ_c) as low as $\leq 1 \times 10^{-9}$ Ωcm^2 [12] are desirable. Consequently, it is imperative to reduce processing thermal budgets and achieve high active carrier concentrations in the S/D. To fulfill these requirements, $Si_{1-x}Ge_x$:P ($x \leq 0.3$) epitaxial growth was performed at temperatures ≤ 500°C using higher order Si and Ge precursors. Low temperature processing typically enables the growth of Si:P with higher active doping concentrations [16-20] and can meet the thermal budget requirements imposed by these advanced architectures. The epitaxial growth of $Si_{1-x}Ge_x$:P ($x \geq 0.3$) has been discussed in Ref. 21,22. However, the active carrier concentration did not exceed ~ 1×10^{20} cm^{-3}. The current study investigates the formation of $Si_{1-x}Ge_x$:P, with lower Ge concentrations ($x \leq 0.3$). The epitaxial growth has been done on blanked Si

wafers with (001) surface orientation. This work aims to assess the achievable maximum active doping concentration and the corresponding lowest contact resistivity, which is the first step in considering this material as a novel nMOS S/D for GAA. This paper is composed of three main sections dedicated to (1) undoped SiGe epi with low %Ge, (2) P doping in epitaxial SiGe:P, and (3) the evaluation of resulting contact resistivities.

2. Experimental methods

The deposition of all layers was executed on 300 mm p-type Si(100) wafers utilizing an Intrepid XP™ epitaxy tool, which is a reduced-pressure chemical vapor deposition system optimized for industrial applications. To enable $Si_{1-x}Ge_x$ epitaxial growth on the blanket silicon wafers, an in-situ thermal treatment was performed in hydrogen (H_2) at 1050°C to eliminate native oxides formed on the surface. The experiments were conducted under a reduced pressure of 20 Torr, with H_2 as carrier gas and keeping the H_2 flow at several tens of standard liters per minute (slm). Disilane (Si_2H_6) and trisilane (Si_3H_8) were used as silicon precursors and combined with digermane (Ge_2H_6, 1% in H_2) and phosphine (PH_3, 15% in H_2) for the growth. This work follows initial developments published in Ref. 21, where similar growth chemistries have been considered. In the current work $Si_{1-x}Ge_x$:P with lower Ge concentrations are being studied. The growth temperature has been varied between 400 and 500°C. The purity of H_2, Si_2H_6, Si_3H_8, Ge_2H_6 and PH_3 gases are 99.9999%, >99,998%, > 99.00%, >99.999 % and >99.999 %.

High-Resolution X-ray Diffraction (HRXRD) and Reflectivity (XRR) measurements were conducted using a JVX7300LM instrument to determine apparent Ge contents and layer thicknesses. The total Ge and P chemical concentrations were quantified through Secondary Ion Mass Spectrometry (SIMS). Active carrier concentrations were evaluated by Micro-Hall Effect measurements (MHE) on a CAPRES CIPTech® M300 tool. Note that all values assume a Hall scattering factor (HSF) of 1. Top view Scanning Electron

Microscopy (SEM) and cross-section Transmission Electron Microscopy (TEM) were used to investigate the sample morphologies and material crystallinity. The Multi-Ring Circular Transmission Line Method (MR-CTLM) was used for ρ_c evaluation of blanket Ti / (Si:P) / $Si_{1-x}Ge_x$:P stacks [12, 23].

3. Results and discussion

3.1 Low temperature growth of undoped SiGe with low Ge content

First, undoped SiGe process conditions were developed to achieve $Si_{1-x}Ge_x$ growth with $x \leq 30\%$. Previous growth studies presented in Ref. 24 were used as a starting point. Figure 1 shows the dependence of Ge contents and growth rates for SiGe layers grown at different temperatures on the Si_2H_6/Ge_2H_6 flow ratio. The Ge content decreases with increasing process temperature, along with the typical trend of decreasing Ge content with increasing Si_2H_6/Ge_2H_6 flow ratio [25]. The growth rate increases with decreasing Si_2H_6/Ge_2H_6 flow ratio, indicating that the decomposition of Ge_2H_6 is the main parameter governing the growth kinetics. As an example, growing $Si_{1-x}Ge_x$ ($x \leq 0.3$) with a Si_2H_6/Ge_2H_6 flow ratio of 333.3 yields an increased growth rate from 0.3 nm/min to 4.4 nm/min with increasing temperature from 400°C to 500°C.

Growth rates in the range of a few Å nm/min are not sufficient for industrial applications. Higher growth rates, in the range of a at least a few nm/min, are necessary. For this reason, a growth temperature of 500°C was selected, in combination with a Si_2H_6/Ge_2H_6 flow ratio of 333.3 since these settings provide sufficiently high growth rates while keeping the overall thermal budget compatible with the researched devices.

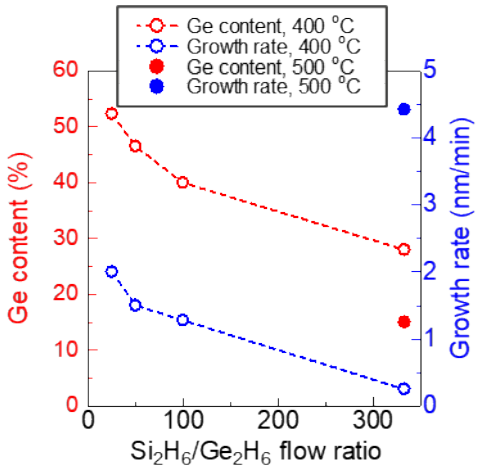

Fig. 1. Apparent Ge contents and growth rate determined from HRXRD as a function of the Si_2H_6/Ge_2H_6 flow ratio at constant Ge_2H_6 flow for undoped SiGe grown at 400°C or 500°C.

Figure 2 displays surface inspection results for $Si_{1-x}Ge_x$ grown with different Si_2H_6/Ge_2H_6 flow ratios. No defects are observed when growing $Si_{0.60}Ge_{0.40}$ at 400°C with a Si_2H_6/Ge_2H_6 flow ratio of 100 (Figure 2(a)). However, defects are observed when using a larger Si_2H_6/Ge_2H_6 flow ratio of 333.3, at the same growth temperature of 400°C (Figure 2(b)) and at a higher growth temperature of 500°C (Figure 2(c)). Defects observed in Figure 2(b) appear smaller compared to those in Figure 2(c) due to the reduced film thickness. These defects are expected to enlarge with increasing film thickness. Still, comparing Figures 2(a) and 2(b), one can observe that Ge-rich layers (Si_2H_6/Ge_2H_6 flow ratios < 100) exhibit no defectivity for the same thickness. However, layers containing a lower Ge content (flow ratios ≤ 333.3) are covered by many defects, for both temperatures evaluated in this work.

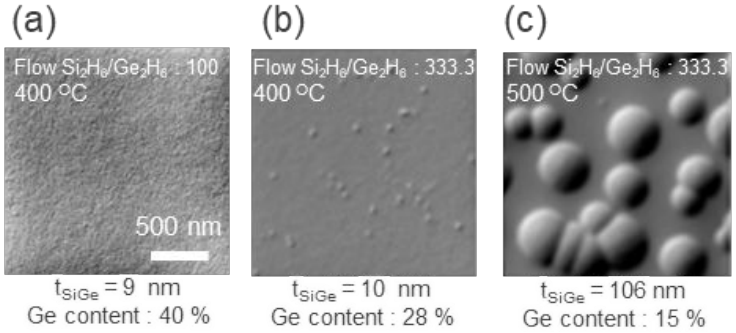

Fig. 2. Top view SEM images of SiGe layer surfaces for samples grown with (a) a Si_2H_6/Ge_2H_6 flow ratio of 100 and at 400°C, (b) a Si_2H_6/Ge_2H_6 flow ratio of 333.3 and at 400°C, and (c) a Si_2H_6/Ge_2H_6 flow ratio 333.3 and at 500°C. Deposition times were the same for all layers.

The TEM cross-section image of such a defect is shown in Figure 3. Defects have a conical shape and contain 2 different regions ascribed to polycrystalline and amorphous phases. The growth rate of the nucleated polycrystalline and amorphous phases is higher than that of the mono-crystalline phase. Such characteristics remind results presented in earlier literature reports. It has e.g., been suggested that such particles may be formed by contamination of available surface sites [24]. However, it appeared that some particles are generated during the growth process and are not formed at the SiGe:P / Si substrate interface. Aubin et al. [26] previously reported on the observation of similar defects when using excessive Si_2H_6 flow rates. The formation of these defects was ascribed to the insufficient surface diffusion of the reacting molecules. Similar phenomena were also observed for Si (or SiGe) epitaxy using Si_2H_6 (and GeH_4) at 20 Torr and low temperature [27], suggesting again gas phase nucleation and low adatom mobility as parameters generating defectivity.

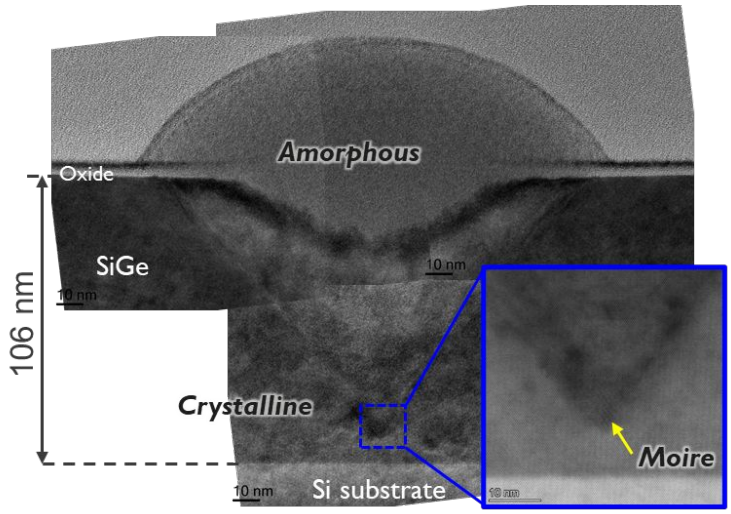

Fig. 3. Bright field cross-section TEM of the $Si_{0.85}Ge_{0.15}$ layer shown in Fig. 2(c) and grown with a Si_2H_6/Ge_2H_6 flow ratio of 333.3 with a focus on a defect. The inset circled in blue corresponds to a zoomed-in image taken at the base of the defect.

3.2 Maximizing active P doping in epitaxial $Si_{1-x}Ge_x$:P with low Ge contents.

It has been reported that the active carrier concentration in $Si_{1-x}Ge_x$:P with x = 40-50% saturates at approximately 1×10^{20} cm^{-3} [21]. To employ this material as a S/D layer, achieving higher active carrier concentrations is imperative. P doping was implemented using process conditions providing sufficiently high growth rates and for Ge contents below 30%. Conditions developed for undoped SiGe and using a Si_2H_6/Ge_2H_6 flow ratio of 333.3 and a growth temperature of 500°C were selected. As shown in Figure 4, the surface morphology significantly improves with increasing PH_3 flow rate, with the disappearance of the observed surface defects. Interestingly, a similar trend was observed in Ref. 28, where originally observed defects disappeared when B_2H_6 was added to the Si_2H_6 + GeH_4 growth chemistry at 450°C. This phenomenon can therefore be attributed

to the promotion of hydrogen desorption from the growth surface thanks to the introduction of PH_3. The presence of phosphorus from PH_3 weakens the Si-H and Ge-H bonds, making it easier for hydrogen to desorb from the surface [29]. This enhances the decomposition of Si_2H_6 as well as SiH_4 molecules, which exhibit low reactivity.

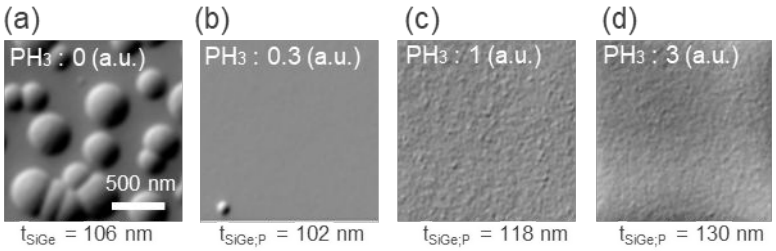

Fig. 4. Top view SEM images showing the morphology of SiGe and SiGe:P films grown with PH_3 flows of (a) 0 a.u., (b) 0.3 a.u., (c) 1 a.u., and (d) 3 a.u.. The Si_2H_6/Ge_2H_6 flow ratio was fixed to 333.3 at 500°C.

Figure 5(a) shows the active carrier concentration ($[P]_{active}$) as estimated from MHE measurements, the total P concentration ($[P]_{total}$) as measured by SIMS, the apparent Ge content as extracted from HRXRD, and the real Ge content as measured by SIMS, all as a function of PH_3 flow. In the low PH_3 flow region (PH_3 flow from 0.3 to 1 a.u.), the Ge concentration decreases rapidly with increasing the PH_3 flow. This dependence is consistent with the one observed in Ref. 21, 25, 28 and suggests a competitive interaction between PH_3 and Ge_2H_6. For PH_3 flows above 1 a.u., the reduction in Ge concentration shows a saturation. This behavior is not yet understood and needs to be studied in more detail.

Increasing the PH_3 flow leads to an increase in active carrier concentration, which reaches a maximum of ~ 2.4×10^{20} cm^{-3}. Subsequently, the active carrier concentration saturates at higher PH_3 flows. This dependence is similar to the one observed in [21]. For PH_3 flows above 1 a.u., $[P]_{total}$ no longer coincides with $[P]_{active}$, suggesting that the P atoms are not fully active but may be present in the layer paired with vacancy defects [9]. Such a large number of substitutional

dopants also affects the strain present in the layer similar to the strain variation as reported for Si:P [9]. This explains the difference in Ge contents as extracted from HRXRD and SIMS. The simultaneous decrease in apparent and total Ge contents in the region up to PH_3 flow = 1 a.u. is therefore, due to the competition between PH_3 and Ge_2H_6 adsorption, and not to strain compensation effects [21, 30]. On the other hand, the decrease in apparent Ge content for a PH_3 flow above 1 a.u., can be partly due to lattice shrinkage caused by P incorporation [30]. This is further illustrated by the Ge content as measured by SIMS, which does not further decrease with increasing PH_3 flow. Nevertheless, further research is needed to understand this mechanism.

Figure 5(b) shows the dependence of the growth rate on PH_3 flow. Growth rates were measured by XRR. The growth rate increased with increasing PH_3 flow rate. A comparable trend was observed for SiGe:B and SiGe:Ga, with these behaviors being ascribed to the increased desorption of surface hydrogen atoms due to interactions with dopants and the creation of active sites that facilitate an effective deposition process [31, 32]. The saturation of $[P]_{active}$ and growth rate with increasing PH_3 flow was observed to be similar to one observed for Si:P with Si_2H_6 grown at 550°C [33]. The stage at which the growth rate plateaus are reached likely coincides with the formation of electrically inactive Si_3P_4, P_3V, or P_4V clusters as the separation between $[P]_{total}$ and $[P]_{active}$ increases [33].

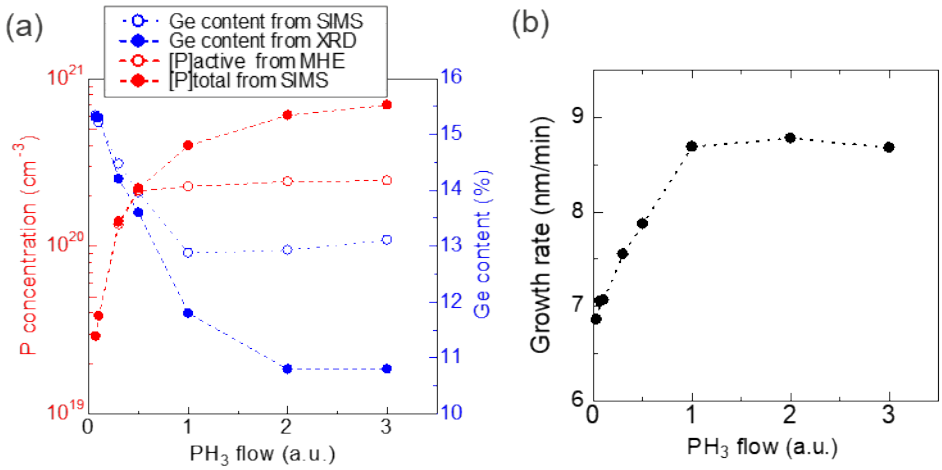

Fig. 5. (a) $[P]_{total}$, $[P]_{active}$, apparent and real Ge contents as a function of the PH_3 flow for layers grown with Si_2H_6/Ge_2H_6 = 333.3 at 500˚C. (b) Corresponding growth rate as a function of PH_3 flow.

3.3 Comparison of $Si_{1-x}Ge_x$:P growth with Si_2H_6 and Si_3H_8

It has been demonstrated that lower growth temperatures may result in the growth of epilayers with higher active carrier concentrations [34]. On the other hand, the decrease in temperature usually leads to a significant reduction in growth rate. A method to maintain acceptable growth rates while using a lower growth temperature involves the use of higher-order precursors such as Si_3H_8 [35-41] . In this section, the properties of $Si_{1-x}Ge_x$:P layers grown with Si_2H_6 and Si_3H_8 will be compared. In addition, the impact of the growth temperature ranging from 450°C to 500°C has been investigated. To ensure a fair comparison, all other SiGe growth conditions were maintained the same.

Figure 6 shows surface morphologies of SiGe:P grown with Si_3H_8 at 450°C and 500°C. As observed previously, defects observed at low PH_3 flows (0.5 a.u. in Figure. 6(a) and (e)), disappear with increasing the PH_3 flow. This is similar to results previously obtained for SiGe:P growth with Si_2H_6 and presented in Figure 4. However, it should be noted that film thicknesses are here lower for

results shown in Figure 4.

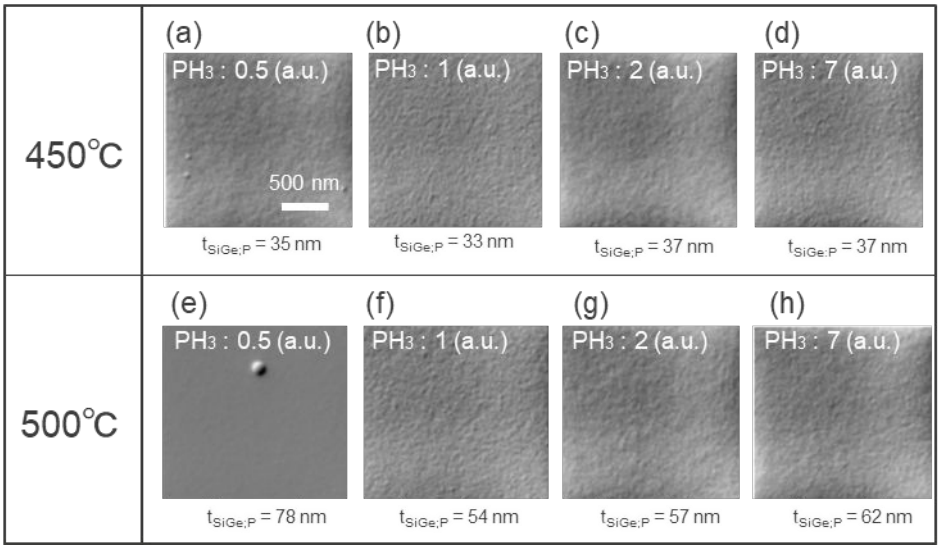

Fig. 6. Top view SEM images showing the morphology of SiGe:P films grown with PH_3 flows of (a) 0.5 a.u., (b) 1 a.u., (c) 2 a.u., (d) 7 a.u. with Si_3H_8/Ge_2H_6 at 450°C, and (e) 0.5 a.u., (f) 1 a.u., (g) 2 a.u., and (h) 7 a.u. with Si_3H_8/Ge_2H_6 at 500°C

Figure 7(a) shows that layers grown with Si_3H_8 exhibit, for a given growth temperature, higher growth rates compared to those grown with Si_2H_6 which is in agreement with literature [24),41)41)]. Si growth using a higher order precursor presents a much more complex growth mechanism than the classical precursors like silane, providing uncommon Arrhenius plots [24),25),38),40)]. Gouyé et al.[38)] proposed descriptions for the decomposition of a higher order Si molecules ending with the direct formation of a Si atom from their gas phase, with SiH_4 molecules as gas by-products. Byeon et al. [41)] proposed two competing reaction schemes providing either Si_2H_6 or SiH_4 as by-products. Alternatively, a specific surface reaction mechanism from Si_3H_8 on H passivated substrates has been proposed by Caymax et al. [39)]. In this model, Si_3H_8 permits the removal of H passivation atoms to open free sites on the growing surface and allowing SiH_3 ligands to bind to it while Si_2H_6 is formed as a by-product. For Si_3H_8, it is

believed that both decomposition mechanisms (in the gas phase and on H passivated surfaces) act together to explain the different Si_3H_8 Arrhenius plots reported in literature [40]. In contrast to conventional precursors, the growth is therefore not limited by H-desorption from the growing surface. This is a main reason why Si_3H_8 enables higher growth rates, in addition to the relatively weaker chemical bonds compared to Si_2H_6, making it easier to decompose at lower temperatures.

At 450°C, the SiGe growth rate using Si_3H_8 is approximately 4 nm/min and it does not show a clear dependency on the PH_3 flow. Although the reduction in growth rate due to the decrease in temperature is noticeable, the precursor therefore still provides an acceptable growth rate. The measured apparent Ge contents as extracted from XRD, are higher for layers grown with Si_3H_8 at 450°C, while they are lower for layers grown with Si_3H_8 at 500°C, compared to layers grown with Si_2H_6 at 500°C, as shown in Figure 7(b). The experimentally observed difference in Ge incorporation for Si_3H_8 vs Si_2H_6 at 500°C is in line with previous studies on epitaxial growth of undoped $Si_{1-x}Ge_x$ using Si_3H_8 /GeH_4 vs SiH_4/GeH_4 [36]. In this work, the difference in Ge incorporation has been assigned to a more efficient Si deposition in case Si_3H_8 is used.

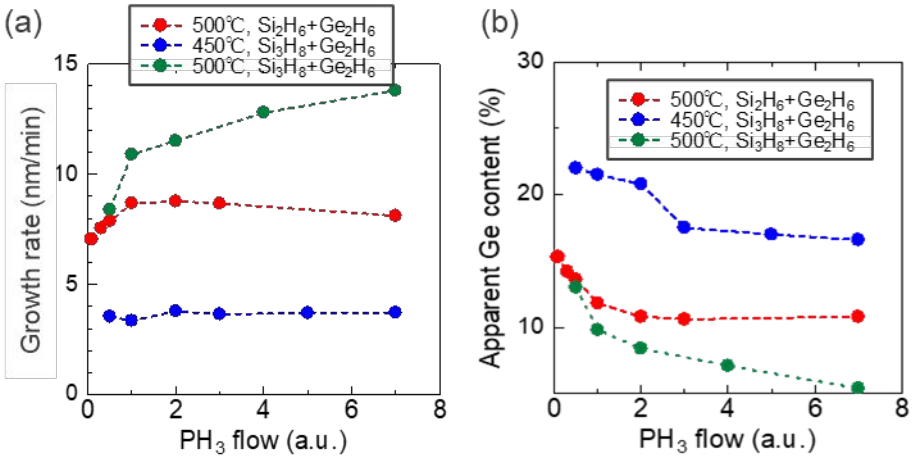

Fig. 7. (a) Growth rates and (b) apparent Ge contents as a function of PH_3 flow for layers grown with Si_2H_6 + Ge_2H_6 at 500°C, Si_3H_8 + Ge_2H_6 at 500°C and 450°C.

The Si_2H_6 and Si_3H_8 flow rates were fixed with Si_2H_6 /Ge_2H_6 and Si_3H_8/Ge_2H_6 ratios of 333.3.

$[P]_{active}$ and $[P]_{total}$ as a function of PH_3 flow rate are shown in Figure 8. For layers grown with Si_3H_8, $[P]_{active}$ saturate at similar values compared to layers grown with Si_2H_6, with a maximum $[P]_{active}$ around ~ 3×10^{20} cm^{-3}. The reduction in growth temperature did therefore not significantly enhance $[P]_{active}$. However, for this set of growth conditions, there might be a PH_3 flow where $[P]_{active}$ shows a maximum, while the layers grown at 500°C show a small but steady increase in $[P]_{active}$ up to the highest PH_3 flow used in this study. On the other hand, the saturation of $[P]_{total}$ seems to vary depending on the choice of the epitaxial growth conditions. Si_3H_8 decomposes more easily than Si_2H_6 and more silicon atoms are supplied to the growth surface. Growing SiGe:P at 450°C with Si_3H_8 tends to enable higher $[P]_{total}$ saturation levels compared to layers grown at 500°C. Comparable $[P]_{active}$ are obtained for the lowest temperature growth with a higher apparent Ge content. This might be beneficial if SiGe:P is considered as lateral stressor grown against nanosheet side walls.

On the other hand, $[P]_{total}$ saturation appears to vary with epi conditions. Si_3H_8 decomposes more readily than Si_2H_6, supplying more silicon atoms to the growth surface and simultaneously incorporating more PH_3 into the layer. At 450°C, using Si_3H_8; leads to higher $[P]_{total}$ than Si_2H_6.

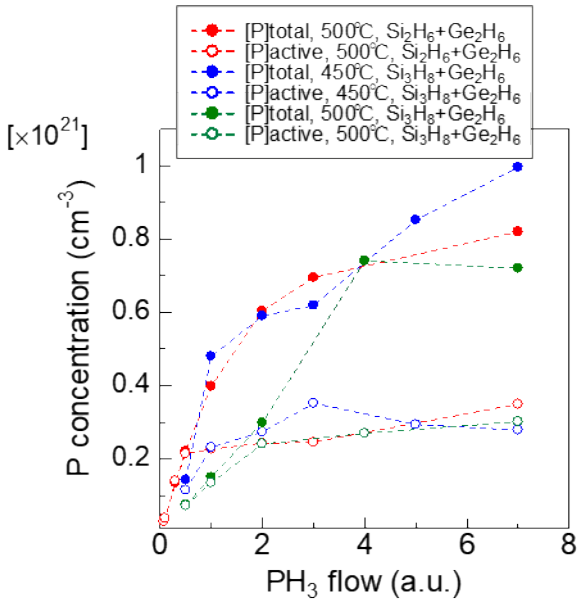

Fig. 8. $[P]_{total}$ and $[P]_{active}$ as a function of the PH_3 flow for $Si_2H_6 + Ge_2H_6$ at 500°C, $Si_3H_8 + Ge_2H_6$ at 450°C and $Si_3H_8 + Ge_2H_6$ at 450°C. Si_2H_6 / Ge_2H_6 and Si_3H_8 / Ge_2H_6 ratios were equal to 333.3.

At the end of this section, Table 1 lists the $Si_{1-x}Ge_x$:P composition, the growth temperature, $[P]_{active}$, $[P]_{total}$ and used precursors obtained in this work and other references. $[P]_{active}$ indicates the highest active concentration reported in each case. For reports where no $[P]_{active}$ are given, the highest $[P]_{total}$ is shown. As can be observed, P concentrations are limited to $1\text{-}3\times10^{20}$ cm^{-3} for layers grown in the reported conditions. Achieving $[P]_{active}$ levels approaching 1×10^{21} cm^{-3} in $Si_{1-x}Ge_x$:P therefore seems challenging. For this reason, additional Si:P capping is considered to improve the contact performance.

Table 1. Characteristics of several $Si_{1-x}Ge_x$:P layers prepared in this work and reported in literature

Ref.	$Si_{1-x}Ge_x$	Temperature(°C)	$[P]_{active}$ (cm^{-3})	$[P]_{total}$ (cm^{-3})	Si precursor	Ge precursor
Ref. 12	Si:P	< 500	1.0×10^{21}	1.5×10^{21}	Si_2H_6	/
This work	$Si_{0.89}Ge_{0.11}$:P	500	2.4×10^{20}	6.0×10^{20}	Si_2H_6	Ge_2H_6
This work	$Si_{0.82}Ge_{0.18}$:P	450	3.0×10^{20}	6.0×10^{20}	Si_3H_8	Ge_2H_6
Ref. 21	$Si_{0.70}Ge_{0.30}$:P	400	1.0×10^{20}	NA	Si_2H_6	Ge_2H_6
Ref. 21	$Si_{0.60}Ge_{0.40}$:P	400	8.0×10^{19}	2.5×10^{20}	Si_2H_6	Ge_2H_6
Ref. 21	$Si_{0.50}Ge_{0.50}$:P	400	6.0×10^{19}	9.0×10^{19}	Si_2H_6	Ge_2H_6
Ref. 22	$Si_{0.56}Ge_{0.44}$:P	650	1.0×10^{20}	NA	SiH_2Cl_2	GeH_4
Ref. 35	$Si_{0.56}Ge_{0.44}$:P	600	NA	2.0×10^{20}	Si_2H_6	Ge_2H_6
Ref. 35	$Si_{0.43}Ge_{0.57}$:P	500	NA	2.0×10^{20}	Si_2H_6	Ge_2H_6

3.4 Specific resistivity of Ti (/ Si:P) / $Si_{1-x}Ge_x$:P contact stacks

The previous sections describe the properties of epitaxial SiGe:P films grown on unpatterned Si(001) surfaces. Lateral S/D growth against the side walls of nanosheet channels is expected to provide the opposite stress sign in the channel in comparison to the more common bottom-up S/D growth [13-14]. The current section will focus on the performance of contact stacks based on SiGe:P and extracted from the CTLM routine. The objective is to assess the potential of SiGe:P as a candidate for the next generation S/D material and to compare the contact properties to those obtained for epitaxial Si:P grown at low temperature [12].

$Si_{1-x}Ge_x$:P ($x \geq 0.3$) layers were grown using the same conditions as those reported in Ref. 21. For these layers, $[P]_{active}$ up to 1×10^{20} cm^{-3} have been measured. The $Si_{0.9}Ge_{0.1}$:P layer has been grown with Si_2H_6/Ge_2H_6 at 500°C using a PH_3 flow of 2 a.u. (Fig. 5(a)). The $Si_{0.82}Ge_{0.18}$:P layer has been grown with Si_3H_8/Ge_2H_6 at 450°C and a PH_3 flow of 2 a.u. (Fig. 8). Finally, a Si:P reference layer was used, with $[P]_{act}$ as high as 1×10^{21} cm^{-3} and grown with the same

growth conditions as reported in Ref. 12.

The CTLM extracted epilayer resistivities are reported in Figure 9(a). The resistivity is lowest for the Ti / 40 nm Si:P sample and is deteriorated with increasing Ge content in $Si_{1-x}Ge_x$:P in Ti / 40 nm $Si_{1-x}Ge_x$:P stacks. This trend correlates with the $[P]_{active}$ for each epi layers. Figure 9(b) shows the corresponding contact resistivities. Low temperature Si:P can yield $[P]_{active}$ as high as 1×10^{21} cm^{-3} and contact resistivities as low as ~ 2×10^{-9} Ωcm^2. For the Ti / 40 nm $Si_{1-x}Ge_x$:P contacts, ρ_c increases with increasing the Ge content. The lowest extracted ρ_c is ~ 2×10^{-8} Ωcm^2 for $Si_{0.89}Ge_{0.11}$:P, which is 10x higher than for Ti / 40 nm Si:P.

The insertion of a thin Si:P layer with a high $[P]_{active}$ in between $Si_{1-x}Ge_x$:P and Ti leads to a significant reduction in ρ_c. Specifically, the ρ_c of Ti / 10 nm Si:P / 40 nm $Si_{0.89}Ge_{0.11}$:P is measured to be ~ 4×10^{-9} Ωcm^2. The ρ_c of Ti / thin Si:P / $Si_{1-x}Ge_x$:P is slightly higher than that of Ti / Si:P and the ρ_c systematically increases with increasing the Ge contents, albeit more gradual than for Ti / $Si_{1-x}Ge_x$:P. A possible consideration is that altering the Ge content in the SiGe:P layer could affect the lattice mismatch between thin Si:P / SiGe:P, potentially affecting Si:P layer relaxation. This increase in ρ_c is however not fully understood and may possibly be caused by other effects. As shown in Figure 10, the surface of thin 10 nm Si:P / 40 nm $Si_{0.5}Ge_{0.5}$:P exhibits a clear cross-hatch pattern (Figure 10(b)), indicative for partial strain relaxation. On the other hand, thin 10 nm Si:P / 40 nm $Si_{0.6}Ge_{0.4}$:P displayed a smooth surface (Figure 10(a)). In other words, increasing the Ge content in $Si_{1-x}Ge_x$:P potentially impacts the contact resistivity due to the induced defectivity caused by the layer relaxation. However, since thin Si:P / SiGe:P with low Ge content did not undergo relaxation, detailed analysis is required to fully understand and clarify these aspects.

Ti / thin Si:P / SiGe:P proves to be a promising approach to mitigate ρ_c penalties while benefiting from correct channel strain. In addition, in transistors, it is essential to also consider S/D resistivity. Nevertheless, this approach may carry significant importance as a mean to enhance mobility by

combining S/D epitaxial stress while achieving low ρ_c.

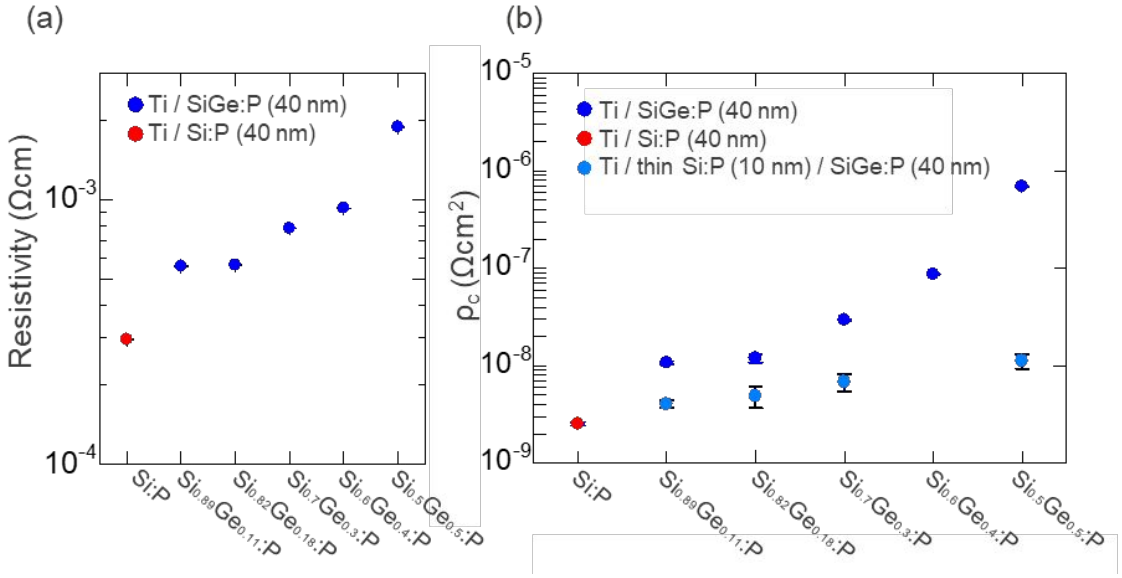

Fig. 9. (a) Resistivity as a function of Ge content for Ti / 40 nm $Si_{1-x}Ge_x$:P and Ti / 40 nm Si:P contact stacks. (b) Specific resistivity of Ti / 40 nm $Si_{1-x}Ge_x$:P, Ti / 40 nm Si:P, and Ti / 10 nm Si:P / 40 nm $Si_{1-x}Ge_x$:P contact stacks as a function of Ge content in $Si_{1-x}Ge_x$:P.

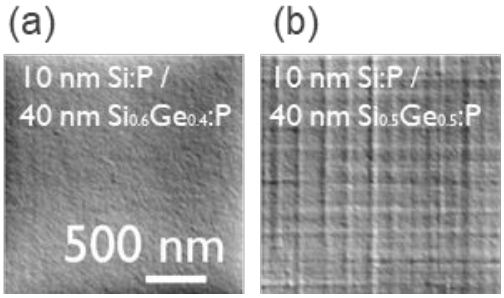

Fig. 10. Top view SEM images showing the morphology of (a) 10 nm Si:P / 40 nm $Si_{0.6}Ge_{0.4}$:P and (b) 10 nm Si:P / 40 nm $Si_{0.5}Ge_{0.5}$:P.

4. Conclusions

This study presents a comprehensive exploration of $Si_{1-x}Ge_x$:P as a new nMOS source/drain (S/D) material for gate-all-around (GAA) transistors in advanced technology nodes beyond 2 nm. The motivation for this work stems from the concern that conventional nMOS S/D materials such as Si:P may cause strain inversion and mobility degradation in modern GAA architectures. This study hence focuses on maximizing active P doping in epitaxial $Si_{1-x}Ge_x$:P with low Ge contents and evaluating the resulting contact properties.

Highly crystalline $Si_{1-x}Ge_x$:P with active carrier concentrations reaching ~ 3.0×10^{20} cm^{-3} was demonstrated, surpassing the limitations observed in previous studies. The optimization of phosphine (PH_3) partial pressure during the growth process plays a crucial role in improving surface morphology and enhancing active carrier concentration. Additionally, switching from Si_2H_6 to Si_3H_8 as silicon precursor confirms higher growth rates, together with advantages in achieving higher active carrier concentrations at lower growth temperatures. Replacing Si:P with $Si_{1-x}Ge_x$:P nevertheless causes some contact performance degradation. However, the incorporation of a thin Si:P layer between the Ti contact and the $Si_{1-x}Ge_x$:P S/D allows to mitigate this effect. Replacing Si:P by SiGe:P S/D in nMOS GAA requires to consider the balance between losses in contact performance vs on current improvement thanks to mobility enhancement. Moreover, if SiGe:P can be expected to be a promising S/D epi for GAA devices, it should be remembered that the S/D must be grown selectively. Given the considered precursor and low temperature process, cyclic deposition/etching routines would be needed. In addition, S/D growth would occur from (110) GAA channel sidewalls rather than on Si(100). This would then require more complex S/D epi optimization. A follow up of this work could also extend the study of low temperature SiGe:P using Si_2H_6 in combination with the more conventional GeH_4, and PH_3.

In summary, $Si_{1-x}Ge_x$:P, with its favorable growth characteristics, relatively high active carrier concentrations and low contact resistivity, emerges as a

promising candidate for nMOS S/D material for GAA architectures to address the evolving demands of sub 2 nm technology nodes. This research opens avenues for further exploration and development in the field of next-generation S/D epitaxial research.

Acknowledgments

The imec core CMOS program members, the European Commission, local authorities, and the imec pilot line are acknowledged for their support.

References

1) E. Capogreco, L. Witters, H. Arimura, F. Sebaai, C. Porret, A. Hikavyy, R. Loo, A. P. Milenin, G. Eneman, P. Favia, H. Bender, K. Wostyn, E. Dentoni Litta, A. Schulze, C. Vrancken, A. Opdebeeck, J. Mitard, R. Langer, F. Holsteyns, N. Waldron, K. Barla, V. De Heyn, D. Mocuta, and N. Collaert, IEEE Transactions on Electron Devices 65 (11), 5145 (2018)

2) G. Yeap, S.S. Lin, Y.M. Chen, H.L. Shang, P.W. Wang, H.C. Lin, Y.C. Peng, J.Y. Sheu, M. Wang, X. Chen, B.R. Yang, C.P. Lin, F.C. Yang, Y.K. Leung, D.W. Lin, C.P. Chen, K.F. Yu, D.H. Chen, C.Y. Chang, H.K. Chen, P. Hung, C.S. Hou, Y.K. Cheng, J. Chang, L. Yuan, C.K. Lin, C.C. Chen, Y.C. Yeo, M.H. Tsai, H.T. Lin, C.O. Chui, K.B. Huang, W. Chang, H.J. Lin, K.W. Chen, R. Chen, S.H. Sun, Q. Fu, H.T. Yang, H.T. Chiang, C.C. Yeh, T.L. Lee, C.H. Wang, S.L. Shue, C.W. Wu, R. Lu, W.R. Lin, J. Wu, F. Lai, Y.H. Wu, B.Z. Tien, Y.C. Huang, L.C. Lu, Jun He, Y. Ku, J. Lin, M. Cao, T.S. Chang, and S.M. Jang, 2019 International Electron Devices Meeting (IEDM), 879 (2019)

3) S. Subramanian, M. Hosseini, T. Chiarella, S. Sarkar, P. Schuddinck, B.T. Chan, D. Radisic, G. Mannaert, A. Hikavyy, E. Rosseel, F. Sebaai, A. Peter, T. Hopf, P. Morin, S. Wang, K. Devriendt, D. Batuk, G. T. Martinez, A. Veloso, E. Dentoni Litta, S. Baudot, Y. K. Siew, X. Zhou, B. Briggs, E. Capogreco, J. Hung, R. Koret, A. Spessot, J. Ryckaert, S. Demuynck, N. Horiguchi, and J. Boemmels, 2020 IEEE Symposium on VLSI Technology, 1 (2020)

4) H. Mertens, R. Ritzenthaler, A. Chasin, T. Schram, E. Kunnen, A. Hikavyy, L.-Å. Ragnarsson, H. Dekkers, T. Hopf, K. Wostyn, K. Devriendt, S. A. Chew, M. S. Kim, Y.

Kikuchi, E. Rosseel, G. Mannaert, S. Kubicek, S. Demuynck, A. Dangol, N. Bosman, J. Geypen, P. Carolan, H. Bender, K. Barla, N. Horiguchi, and D. Mocuta, 2016 IEEE Symposium on VLSI Technology, 158 (2016)

5) S. E. Thompson, M. Armstrong, C. Auth, M. Alavi, M. Buehler, R. Chau, S. Cea, T. Ghani, G. Glass, T. Hoffman, C. H. Jan, C. Kenyon, J. Klaus, K. Kuhn, Z. Ma, B. Mcintyre, K. Mistry, A. Murthy, B. Obradovic, R. Nagisetty, P. Nguyen, S. Sivakumar, R. Shaheed, L. Shifren, B. Tufts, S. Tyagi, and M. Bohr, IEEE Transactions on Electron Devices, 51 (11), 1790 (2004)

6) E. Parton and P. Verheyen, III-Vs Review, 19 (3), 28 (2006)

7) C. Auth, C. Allen, A. Blattner, D. Bergstrom, M. Brazier, M. Bost, M. Buehler, V. Chikarmane, T. Ghani, T. Glassman, R. Grover, W. Han, D. Hanken, M. Hattendorf, P. Hentges, R. Heussner, J. Hicks, D. Ingerly, P. Jain, S. Jaloviar, R. James, D. Jones, J. Jopling, S. Joshi, C. Kenyon, H. Liu, R. McFadden, B. McIntyre, J. Neirynck, C. Parker, L. Pipes, I. Post, S. Pradhan, M. Prince, S. Ramey, T. Reynolds, J. Roesler, J. Sandford, J. Seiple, P. Smith, C. Thomas, D. Towner, T. Troeger, C. Weber, P. Yashar, K. Zawadzki, and K. Mistry, 2012 VLSI Technology Digest of Technical Papers, 131 (2012)

8) H. Wu, O. Gluschenkov, G. Tsutsui, C. Niu, K. Brew, C. Durfee, C. Prindle, V. Kamineni, S. Mochizuki, C. Lavoie, E. Nowak, Z. Liu, J. Yang, S. Choi, J. Demarest, L. Yu, A. Carr, W. Wang, J. Strane, S. Tsai, Y. Liang, H. Amanapu, I. Saraf, K. Ryan, F. Lie, W. Kleemeier, K. Choi, N. Cave, T. Yamashita, A. Knorr, D. Gupta, B. Haran, D. Guo, H. Bu, and M. Khare, 2018 International Electron Devices Meeting (IEDM), 35 (2018)

9) E. Rosseel, S. Dhayalan, A. Hikavyy, R. Loo, H.B. Profijt, D. Kohen, S. Kubicek, T. Chiarella, H. Yu, N. Horiguchi, D. Mocuta, K. Barla, Y. Thean, G. Bartlett, J. Margetis, N. Bhargava, and J. Tolle, ECS Transactions, 75 (8), 347 (2016)

10) H. Mertens, R. Ritzenthaler, A. Hikavyy, M. S. Kim, Z. Tao, K. Wostyn, S. A. Chew, A. De Keersgieter, G. Mannaert, E. Rosseel, T. Schram, K. Devriendt, D. Tsvetanova, H. Dekkers, S. Demuynck, A. Chasin, E. Van Besien, A. Dangol, S. Godny, B. Douhard, N. Bosman, O. Richard, J. Geypen, H. Bender, K. Barla, D. Mocuta, N. Horiguchi, and A.V-Y Thean, 2015 IEEE Symposium on VLSI Technology, 142 (2015)

11) K. Cheng, A. Khakifirooz, P. Kulkarni, S. Ponoth, J. Kuss, D. Shahrjerdi, L. F. Edge, A.

Kimball, S. Kanakasabapathy, K. Xiu, S. Schmitz, A. Reznicek, T. Adam, H. He, N. Loubet, S. Holmes, S. Mehta, D. Yang, A. Upham, S.-C. Seo, J. L. Herman, R. Johnson, Y. Zhu, P. Jamison, B. S. Haran, Z. Zhu, L. H. Vanamurth, S. Fan, D. Horak, H. Bu, P. J. Oldiges, D. K. Sadana, P. Kozlowski, D. McHerron, J. O'Neill, and B. Doris, 2009 IEEE International Electron Devices Meeting (IEDM), 1 (2009)

12) C. Porret, J.-L. Everaert, M. Schaekers, L.-A. Ragnarsson, A. Hikavyy, E. Rosseel, G. Rengo, R. Loo, R. Khazaka, M. Givens, X. Piao, S. Mertens, N. Heylen, H. Mertens, C. Toledo de Carvalho Cavalcante, G. Sterck, S. Brus, A. Nalin Mehta, M. Korytov, D. Batuk, P. Favia, R. Langer, G. Pourtois, J. Swerts, E. Dentoni Litta, and N. Horiguchi, 2022 International Electron Devices Meeting (IEDM), 34 (2022)

13) G. Eneman, A. Veloso, P. Favia, A. Hikavyy, C. Porret, H. Arimura, A. D. Keersgieter, G. Pourtois, R. Loo, A. Spessot, P. Matagne, J. Ryckaert, and N. Horiguchi, IEEE Electron Device Lett., 38, 5 (2017)

14) G. Eneman, A. Veloso, P. Favia, A. Hikavyy, C. Porret, H. Arimura , A. D. Keersgieter, G. Pourtois, R. Loo, A. Spessot, P. Matagne, J. Ryckaert, and N. Horiguchi, ECS Trans, 98 (5), 253 (2020)

15) A.Vandooren, Z. Wu, N. Parihar, J. Franco, B. Parvais, P. Matagne, H. Debruyn, G. Mannaert, K. Devriendt, L. Teugels, E. Vecchio, D. Radisic, E. Rosseel, A. Hikavyy, B. T. Chan, N. Waldron, J. Mitard, G. Besnard, A. Alvarez, G. Gaudin, W. Schwarzenbach, I. Radu, B.-Y. Nguyen, K. Huet, T. Tabata, F. Mazzamuto, S. Demuynck, J. Boemmels, N. Collaert, and N. Horiguchi, 2020 IEEE Symposium on VLSI Technology, 1 (2020)

16) J. Kanyandekwe, M. Bauer, T. Marion, L. Saidi, J. Pin, J. Bisserier, J. Richy, N. Gauthier, P. Dezest, L. Brunet, V. Lapras, T. Dewolf, S. Thomas and J.M. Hartmann, ECS Trans., 109 (4), 121 (2022)

17) R. Khazaka, L. Lima, E. Rosseel, A. Hikavyy, V. Costa, and Q. Xie, Electrochemical Society Meeting Abstracts prime2020. The Electrochemical Society, Inc., 1734 (2020).

18) E. Rosseel, C. Porret, A. Hikavyy, R. Loo, M. Tirrito, B. Douhard, O. Richard, N. Horiguchi, and R. Khazaka, ECS Trans., 98 (5), 37 (2020)

19) H. Yu, M. Schaekers, E. Rosseel, A. Peter, J.-G. Lee, W.-B. Song, S. Demuynck, T. Chiarella, L-Å. Ragnarsson, S. Kubicek, J. Everaert, N. Horiguchi, K. Barla, D. Kim, N. Collaert, A. V. –Y. Thean, and K. De Meyer, ECS Trans, 64 (6), 959 (2014)

20) E. Rosseel, H. Benjamin Profijt, A. Hikavyy, J. Tolle, S. Kubicek, G. Mannaert, C. L'abbe, K. Wostyn, N. Horiguchi, T. Clarysse, B. Parmentier, S. Dhayalan, H. Bender, J. W. Maes, S. Mehta, and R. Loo, ECS Trans., 64 (6), 977 (2014)

21) A. Hikavyy, C. Porret, A. Vohra, M. Ayyad, B. Douhard, and R. Loo, ECS Trans., 98 (5), 43 (2020)

22) J. M. Hartmann, M. Py, J.P. Barnes, B. Prévitali, P. Batude, and T. Billon, Journal of Crystal Growth, 327 (1), 68 (2011)

23) H. Yu, M. Schaekers, T. Schram, E. Rosseel, K. Martens, S. Demuynck, N. Horiguchi, K. Barla, N. Collaert, K. De Meyer, and A. Thean, IEEE Electron Device Lett., 36 (6), 600 (2015)

24) A. Hikavyy, I. Zyulkov, H. Mertens, L. Witters, R. Loo, and N. Horiguchi, Mater. Sci. Semicond. Process., 70 (1), 24 (2017)

25) J. M. Hartmann, J. Aubin, and J. P. Barnes, ECS Transactions, 75 (8), 281 (2016)

26) S. K. Dhayalan, R. Loo, A. Hikavyy, E. Rosseel, H. Bender, O. Richard, and W. Vandervorst, Journal of Crystal Growth 426, 75 (2015)

27) J. Aubin, J.M. Hartmann, and V. Benevent, Thin Solid Films 602, 36 (2016)

28) J. Aubin, J. M. Hartmann, M. Veillerot, Z. Essa, and B. Sermage, Semicond. Sci. Technol. 30 115006 (2015)

29) J. Vizoso, F. Martín, J. Suñé, and M. Nafría, Appl. Phys. Lett. 70, 3287 (1997)

30) K.D. Weeks, S.G. Thomas, P. Dholabhai, and J. Adams., Thin Solid Films 520, 3158 (2012).

31) G. Rengo, C. Porret, A. Hikavyy, G. Coenen, M. Ayyad, R. Morris, S. Pollastri, D. Souza, D. Grandjean, R. Loo, and A. Vantomme, ECS Transactions 109 (4), 249 (2022)

32) A. Hikavyy, C. Porret, R. Loo, M. Mencarelli, P. Favia, M. Ayyad, B. Briggs, R. Langer, and N. Horiguchi, ECS Trans. 104 (4), 139 (2021)

33) J.M. Hartmann and J. Kanyandekwe, Journal of Crystal Growth 582, 126543 (2022)

34) N.D. Nguyen, R. Loo, and M. Caymax, Applied Surface Science 254 (19), 6072 (2008)

35) S. Wirths, D. Buca, A.T. Tiedemann, P. Bernardy, B. Holländer, T. Stoica, G. Mussler, U. Breuer, and S. Mantl, Solid-State Electronics 83, 2 (2013)

36) S. Takeuchi, N. D. Nguyen, J. Goosens, M. Caymax, and R. Loo, Thin Solid Film 518, 18 (2010)

37) J. G. Martin, H. E. O'Neal, and M. A. Ring, International journal of chemical kinetics 22 (6), 613 (1990)

38) A. Gouyé, O. Kermarrec, A. Halimaoui, Y. Campidelli, D. Rouchon, M. Burdin, P. Holliger, and D. Bensahel, Journal of Crystal Growth 311, 3522 (2009)

39) M. Caymax, F. Leys, J. Mitard, K. Martens, L. Yang, G. Pourtois, W. Vandervorst, M. Meuris, and R. Loo, Journal of The Electrochemical Society 156 (12), H979 (2009)

40) B. Vincent, R. Loo,W. Vandervorst, G. Brammertz, and M. Caymax, Journal of Crystal Growth 312, 2671 (2010)

41) D.-S. Byeon, Y. Choi, C. Cho, D. Yoon, K. Lee, S. Baik, and D.-H. Ko, Journal of the Korean Physical Society 78, 712 (2021)